

# Frequency-Controlled Thermalization Phase Transition in a Chaotic Periodically-Driven Classical Spin Chain

Owen Howell,<sup>1,\*</sup> Phillip Weinberg,<sup>1</sup> Dries Sels,<sup>1,2,3</sup> Anatoli Polkovnikov,<sup>1</sup> and Marin Bukov<sup>4,†</sup>

<sup>1</sup>*Department of Physics, Boston University, 590 Commonwealth Ave., Boston, MA 02215, USA*

<sup>2</sup>*Department of Physics, Harvard University, 17 Oxford st., Cambridge, MA 02138, USA*

<sup>3</sup>*Theory of quantum and complex systems, Universiteit Antwerpen, B-2610 Antwerpen, Belgium*

<sup>4</sup>*Department of Physics, University of California, Berkeley, CA 94720, USA*

(Dated: January 11, 2023)

We reveal a novel continuous dynamical heating transition between a prethermal and an infinite-temperature phase in a clean, chaotic periodically-driven classical spin chain. The transition time is a steep exponential function of the driving frequency, showing that the exponentially long-lived prethermal plateau, originally observed in quantum Floquet systems, survives the classical limit. Despite the inapplicability of Floquet's theorem to nonlinear systems, we present strong evidence that the physics of the prethermal phase is described well by the inverse-frequency expansion, even though its stability and robustness are related to drive-induced coherence not captured by the expansion. Our results pave the way to transfer the ideas of Floquet engineering to classical many-body systems, and are directly relevant for cold atom experiments in the superfluid regime.

Periodically-driven systems are currently experiencing an unprecedented revival of interest through theoretical and experimental design of novel states of matter. Commonly known as *Floquet engineering*, this approach has enjoyed success in the regime of high driving frequency, where it has been appreciated as a useful tool to ascribe novel properties to otherwise trivial static Hamiltonians [1–3]. Prominent examples include the Kapitza pendulum [4], cold-atom realisations of topological [5–12] and spin-dependent [13] bands, artificial gauge fields [14–21], spin-orbit coupling [22, 23], enhanced magnetic correlations [24], synthetic dimensions [25–27], and photonic topological insulators [28–30].

The applicability of Floquet engineering requires the ability to prepare the periodically driven system in the corresponding Floquet state [31–33], and the stability of the system to detrimental heating [34, 35]. Presenting a major bottleneck at the forefront of present-date experimental research, heating processes play an important role in many-body Floquet systems, and understanding the underlying physics is expected to offer significant advances in the field. Unlike single-particle quantum systems, such as the kicked rotor [36] and bosonic band models [37, 38], it is commonly believed that generic isolated clean periodically-driven quantum many-body systems heat up to an infinite-temperature state [39–43]. Nonetheless, heating rates have been shown to be at least exponentially suppressed in the drive frequency [44, 45].

In this paper, we present a state-of-the-art numerical study of thermalisation in a clean, globally-driven, isolated *classical* spin chain, reaching times beyond the astronomical  $10^{10}$  driving cycles. We find that, the dynamics falls into four stages, see Fig. 1: an initial transient (i) during which the system exhibits *constrained* ther-

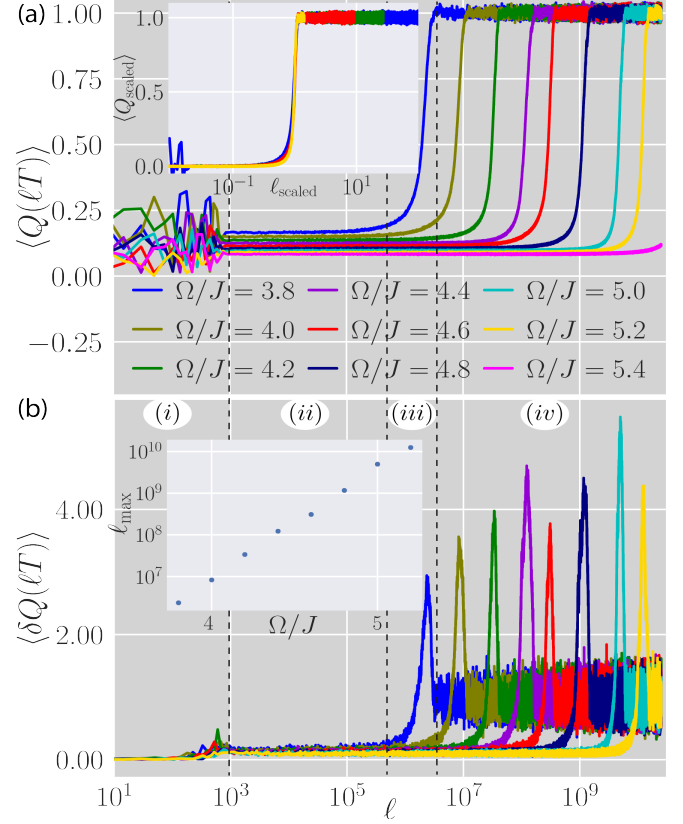


FIG. 1: Noise-averaged energy (a) and energy variance (b) as a function of the number of driving cycles  $\ell$ . Insets: rescaled energy curves (a) by the position of the peak in the variance curves (b), reveal a dynamical heating transition from a prethermal phase to an infinite-temperature phase in the limit  $\Omega, \ell \rightarrow \infty$ . The dashed vertical lines mark the four stages of evolution for  $\Omega/J = 3.8$  [see text]. See Fig. 2 for parameters.

\*Electronic address: [olh20@bu.edu](mailto:olh20@bu.edu)

†Electronic address: [mgbukov@berkeley.edu](mailto:mgbukov@berkeley.edu)

malization to a finite energy density set by the initial ensemble, (ii) a frequency-controlled long-lived prether-

mal phase [44, 46, 47] ideally suited for Floquet engineering, followed by (iii) a late crossover governed by *unconstrained* thermalisation to (iv) a featureless infinite-temperature state. Our analysis reveals the existence of a dynamical continuous phase transition between a prethermal phase and an infinite-temperature phase at infinite times and infinite drive frequencies. Focusing on the prethermal phase, we demonstrate that a key role for its exponentially long duration is played by drive-induced coherence. In particular, stopping the periodic drive and then restarting it allows the system to dephase and leads to a strong increase of the heating rate. The prethermal phase is captured well by the inverse-frequency expansion originally developed for quantum systems, which allows to transfer the machinery of Floquet engineering directly to classical many-body systems despite the absence of a Floquet theorem for nonlinear equations of motion.

From a classical mechanics perspective, we analyze the time scales for the system to leave a small corner of phase space around the initial state and exhibit chaotic behaviour, thereby heating up to an infinite-temperature state. A related question was addressed in a pioneering numerical study by Fermi, Pasta, Ulam and Tsingou, which gave evidence for a parametrically slow thermalisation in a system of coupled classical oscillators [48, 49], puzzling the community for the past few decades. Theorems in Hamiltonian mechanics have been proved, showing that the motion of action variables in nearly-integrable Hamiltonian systems remains confined to a small region of phase space until exponentially long times, controlled by the integrability breaking parameter [50–52]. This behaviour is accompanied by subdiffusion, as reported for a system of periodically-kicked coupled pendula [53, 54]. The chaotic many-body dynamics of periodically-kicked spin chains has been studied using a classical Loschmidt echo approach [55, 56].

*Model.*—Consider a classical Ising chain with periodic boundary conditions, described by the energy function

$$H(t) = \begin{cases} \sum_{j=1}^N JS_j^z S_{j+1}^z + hS_j^z & \text{for } t \in [0, T/2] \bmod T \\ \sum_{j=1}^N gS_j^x & \text{for } t \in [T/2, T] \bmod T \end{cases}$$

where  $J$  denotes the nearest-neighbour interaction strength, while  $h$  and  $g$  are the magnetic field strengths along the  $z$  and  $x$ -directions, respectively. The spin [or rotor] variable  $\vec{S}_j$ ,  $|\vec{S}_j| = 1$ , on site  $j$  satisfies the Poisson bracket relation  $\{S_i^\mu, S_j^\nu\} = \delta_{ij} \varepsilon^{\mu\nu\rho} S_j^\rho$ , with  $\varepsilon^{\mu\nu\rho}$  the fully antisymmetric tensor.

The time dependence arises due to periodic switching of two time-independent Hamilton functions, for a duration of  $T/2$  each, with frequency  $\Omega = 2\pi/T$ . The time evolution of the system is governed by Hamilton's EOM  $\dot{S}_j^\mu(t) = \{S_j^\mu, H(t)\}$ . Interested in the long-time thermalisation properties, we focus on stroboscopic evolution. Integrating the EOM over the total period  $T$ , the evolved state is obtained from a successive application of a discrete map  $\vec{S}_j(\ell T) = [\tau_2 \circ \tau_1]^\ell(\vec{S}_j(0))$ , with  $\ell \in \mathbb{N}$  counting the driving cycles. During the first half-

period, the time evolution follows the *non-linear* rotation  $\tau_1$  about  $z$ -axis:

$$\tau_1(\vec{S}_j) = \begin{bmatrix} S_j^x \cos(\kappa_j T/2) - S_j^y \sin(\kappa_j T/2) \\ S_j^x \sin(\kappa_j T/2) + S_j^y \cos(\kappa_j T/2) \\ S_j^z \end{bmatrix} \quad (1)$$

with spin-dependent natural frequency of rotation  $\kappa_j = J(S_{j-1}^z + S_{j+1}^z) + h$ . The dynamics in the second half-period follows the rotation  $\tau_2$  about the  $x$ -axis:

$$\tau_2(\vec{S}_j) = \begin{bmatrix} S_j^x \\ S_j^y \cos(gT/2) - S_j^z \sin(gT/2) \\ S_j^y \sin(gT/2) + S_j^z \cos(gT/2) \end{bmatrix} \quad (2)$$

The map  $\tau_2 \circ \tau_1$  is the classical analogue of the quantum Floquet unitary.

Motivated by experiments which study Floquet-engineered ordered low-energy states at high drive frequencies, we prepare the system at time  $t = 0$  in the lowest-energy state (a.k.a. the ground state, GS) of the time-averaged Hamiltonian

$$H_{\text{ave}} = \frac{1}{2} \sum_{j=1}^N JS_j^z S_{j+1}^z + hS_j^z + gS_j^x, \quad (3)$$

with energy density  $E_{\text{GS}}/N \approx -1.235$ . Whenever  $J, h, g$  have equal sign and are of the same order of magnitude, the GS features antiferromagnetic (AFM) order w.r.t. a direction in the  $xz$ -plane, parametrized by the azimuthal angle  $\theta$ . Making use of translational invariance, one can determine the value of  $\theta$  which minimizes the energy  $E_{\text{GS}}(\theta)$ . Translational invariance constrains the GS dynamics to be uniquely described by two coupled spin degrees of freedom, corresponding to the AFM unit cell. To bring out the many-body character of the model, we add small noise to the azimuthal angle of each spin, independently drawn from a uniform distribution over  $[-\pi/100, \pi/100]$ , which breaks translational symmetry and allows for thermalisation. The quantities we consider are averaged over an ensemble of 100 noisy initial state realizations. We verified that the long-time dynamics is independent of the strength of the noise [57], provided the latter remains small, and does not significantly change the energy of the initial state. In the following, we denote by  $\langle \cdot \rangle$  the average over the ensemble of noise realizations.

*Heating Transition.*—Compared to classical systems, studies on thermalising dynamics in quantum models feature some deficiencies, due to left-over finite-size effects inherent to state-of-the-art exact diagonalization simulations: Since energy absorption is known to happen through Floquet many-body resonances [58–60], (i), their density depends strongly on the drive frequency at any fixed many-body bandwidth. As the bandwidth scales linearly with the system size  $N$ , this puts an upper bound on  $\Omega$  for the system to be in the many-body regime. This also limits the occurrence of higher-order absorption processes, reducing the overall capacity for energy

absorption. (ii) Low-energy initial states, whose energy level spacing does not follow the  $2^{-N}$  scaling of the bulk, further restrict the appearance of resonances. However, these issues are intrinsic to quantum models and none of them is problematic in periodically-driven classical systems. The classical energy manifold is continuous allowing for excitations at all energies, and one can easily reach system sizes of several hundred spins, which mitigates the constraint on the reliable upper bound for the driving frequency by a few orders of magnitude. Nevertheless, studying classical systems comes at a notable price: one cannot access the infinite-time behavior, and is thus limited to finite [though typically sufficiently large for all experimental purposes] times.

Often times experiments in Floquet engineering are designed to study the GS of the infinite-frequency Hamiltonian (3). Therefore,  $H_{\text{ave}}$  constitutes a natural observable to measure the excess energy pumped into the system from the drive. Let us define the dimensionless expected energy and energy variance [58], over the initial ensemble of noisy AFM states:

$$\langle Q(\ell T) \rangle = \frac{\langle H_{\text{ave}}[\{\vec{S}_j(\ell T)\}] \rangle - E_{\text{GS}}}{\langle H_{\text{ave}} \rangle_{\beta=0} - E_{\text{GS}}} \in [0, 1], \quad (4)$$

$$\langle \delta Q(\ell T) \rangle = \sqrt{\frac{\langle H_{\text{ave}}^2[\{\vec{S}_j(\ell T)\}] \rangle - \langle H_{\text{ave}}[\{\vec{S}_j(\ell T)\}] \rangle^2}{\langle H_{\text{ave}}^2 \rangle_{\beta=0} - \langle H_{\text{ave}} \rangle_{\beta=0}^2}}.$$

The normalization is chosen w.r.t. an infinite-temperature ensemble, where each spin points at a random direction, and hence  $\langle H_{\text{ave}} \rangle_{\beta=0} = 0$  and  $\langle H_{\text{ave}}^2 \rangle_{\beta=0} = N/3(J^2/3 + h^2 + g^2)$ . Initializing the system in the ensemble of noisy AFM states, we have  $\langle Q(\ell T) \rangle \approx 0$  if the system does not absorb energy, and  $\langle Q(\ell T) \rangle = 1$  whenever the drive heats up the ensemble to infinite temperature.

There are four stages in the evolution of the system, see Fig. 1. Notice that the time between the pre-thermal plateau and the infinite-temperature state in stage (iii), corresponding to maximum energy variance:  $\ell_{\text{max}}(\Omega) = \arg\max_{\ell} \langle \delta Q(\ell T) \rangle$ , scales *exponentially* [61] with the driving frequency  $\Omega$ , c.f. Fig. 1b (inset). Thus, we can rescale the  $\langle Q(\ell T) \rangle$  curves with respect to the energy in the beginning of the prethermal phase (ii):

$$\langle Q_{\text{scaled}}(\ell_{\text{scaled}} T) \rangle = \frac{\langle Q(\ell_{\text{scaled}} T) \rangle - \langle Q \rangle_{\text{prethermal}}}{\langle Q \rangle_{\beta=0} - \langle Q \rangle_{\text{prethermal}}}, \quad (5)$$

where  $\ell_{\text{scaled}} = \ell/\ell_{\text{max}}(\Omega)$ . Figure 1a (inset) shows the collapse in the energy absorption curves with increasing frequency, whereas the width of the peak in  $\delta Q(\ell_{\text{scaled}})$  stays constant [57]. The physics of the dynamical thermalization transition resembles striking similarities with the phase transition observed in the 1d Ising model at zero temperature, where the squared magnetization plays the role of energy absorption, while drive frequency and time are analogous to inverse temperature and system size, respectively [57]. This suggests that heating happens through a continuous phase transition in the limit

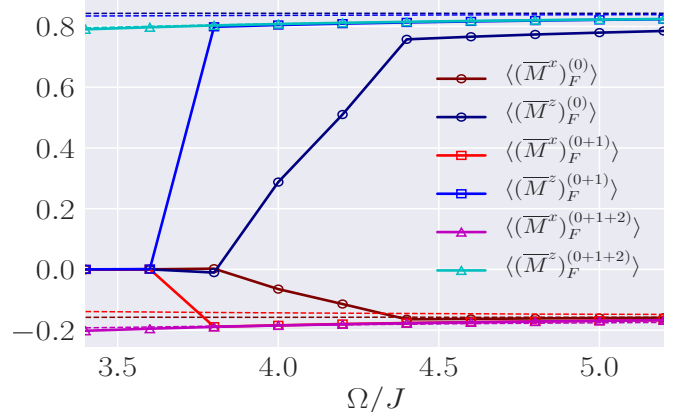


FIG. 2: Staggered magnetization  $\langle \overline{M}^\alpha \rangle_F^{(0+1+\dots+m)}$  in the prethermal phase to different order  $m$  in the ME (solid lines), compared to its value in the initial GS of the corresponding Floquet Hamiltonian (dashed). The parameters are  $g/J = 0.9045$ ,  $h/J = 0.809$ ,  $N_T = 10^6$ , and  $N = 100$ . Every point is averaged over an ensemble of 100 noise realisations.

$\Omega, t \rightarrow \infty$ . At moderate frequencies and times relevant for experiments, we find a sharp crossover instead.

*Prethermal Phase.*—The prethermal plateau plays a crucial role in strongly-interacting systems because it offers a stable window to experimentally realize novel many-body states of matter. We demonstrate that the inverse-frequency expansion can be used to gain a better understanding of the prethermal phase, and present compelling evidence that the phase is captured by a *local* effective Hamilton function, amenable to Floquet engineering, even in chaotic classical many-body systems.

Even though Floquet theory does not apply to non-linear EOM, a Magnus expansion (ME) can be formally defined for classical systems by replacing commutators with Poisson brackets [3, 62]. However, this should be approached with care, as it is an open question if and why such a procedure should work. On one hand stands the notable application of the ME to the Kapitza pendulum [3, 42, 62], on the other – the recent finding that the ME does not capture resonances, which renders its convergence at most asymptotic [32, 58, 60].

To show the applicability of the ME, note that experiments prepare the Floquet-engineered initial state at finite frequencies, rather than the GS of the infinite-frequency Hamiltonian  $H_{\text{ave}} = H_F^{(0)}$ . This corresponds to initializing the dynamics in the GS of the exact Floquet Hamiltonian  $H_F \approx H_F^{(0+\dots+m)} \sim \mathcal{O}(\Omega^{-m})$ , whose approximation we compute to a given order  $m$  in ME [57].

While energy is the most natural observable to study heating, it typically cannot be measured directly in experiments. We now argue that the prethermal phase affects also generic local observables. Consider the stag-

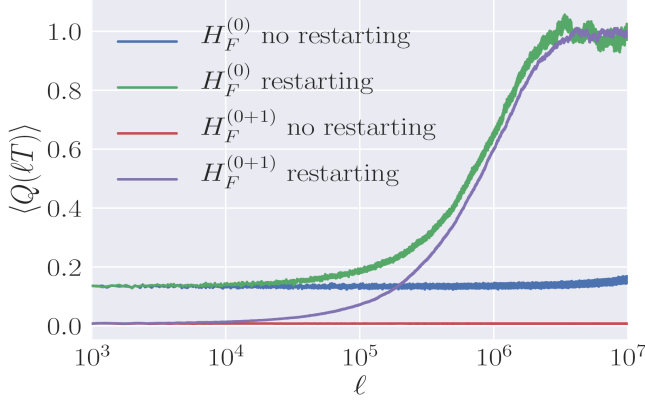


FIG. 3: Comparison of behavior of  $H_F^{(0)}$  and  $H_F^{(0+1)}$  with and without “restarting” as a function of the number of driving cycles  $\ell$ , for  $\Omega/J = 4.2$ . The restarting process is done every 1000 periods. The allowed errors in energy and variance of the new and old ensembles were chosen to be less than  $0.005J$ . See Fig. 2 for parameters.

gered magnetization and its long-time average

$$M^\alpha(\ell T) = \frac{1}{N} \sum_{j=1}^N (-1)^j S_j^\alpha(\ell T); \overline{M}^\alpha = \frac{1}{N_T} \sum_{\ell=N_T}^{N_T+10^3} M^\alpha(\ell T),$$

where  $N_T$  denotes a large number of driving cycles. This observable is an order parameter for AFM correlations, and its time dependence measures how well the system retains the initial AFM structure. Figure 2 (circles) shows the components of the time-averaged magnetisation  $\overline{M}^\alpha$  as a function of frequency to order  $m=0$ . For  $\Omega \lesssim \Omega_*$ , where  $\Omega_*$  is the crossover frequency, the system enters quickly the infinite-temperature phase, and all information about the initial state is lost:  $\overline{M}^\alpha = 0$ . However, in the long-lived prethermal phase  $\Omega \gtrsim \Omega_*$ , much of the AFM correlations are preserved. The corresponding dashed lines show the staggered magnetization of the initial state, which is approached in the limit  $\Omega/J \rightarrow \infty$ .

This raises the intriguing question whether one can use Floquet engineering to control expectation values of observables in the prethermal phase. Upon increasing the order of the ME, we find a significant improvement between the staggered magnetization of the initial ensemble and its time-averaged value in the pre-thermal plateau (squares, triangles), cf. Fig. 2. This implies that one can successfully Floquet-engineer the behavior of observables in the prethermal phase. This is remarkable and rather unexpected, since there is no version of Floquet’s theorem for nonlinear EOM. Such a behavior likely originates from the emergent quasiconserved local integrals of motion for  $\Omega \lesssim \Omega_*$ .

Prethermal Floquet phases are often assumed to be featureless states which are stroboscopically equivalent to thermal equilibrium with respect to the local Floquet Hamiltonian. We now show that this assumption

is incomplete: the prethermal phase is fused by drive-induced coherence which is responsible for their exponentially long stability. To demonstrate this, we compare the exact Floquet evolution, with an evolution where we periodically restart the dynamics from the thermal Gaussian ensemble of  $H_F^{(0)}$ , with mean energy and width chosen to match those of the time evolved initial ensemble into the prethermal phase. We call this process “restarting”. Figure 3 shows a comparison of the expected values of  $H_F^{(0)}$ , following the uninterrupted (blue) and “restarting” evolution (green). The “restarting” procedure was applied every  $10^3$  cycles to prevent the system from re-synchronizing. As a result, the restarted dynamics enters the infinite-temperature phase exponentially earlier. The increase of energy caused by “restarting” suggests that the prethermal phase contains additional very slow coherent dynamics, perhaps the classical analogue of many-particle Rabi-type oscillations as observed in small quantum systems [58], which serves as a glue for the prethermal state. To argue that the prethermal phase is a property of the time-evolved ensemble and not of the Gaussian energy ensemble used for “restarting”, we fix the initial ensemble of noisy AFM states based on the GS of  $H_{\text{ave}} = H_F^{(0)}$ , and repeat the procedure measuring  $H_F^{(0+1)}$ , c.f. Fig 3. As expected, this affects the energy density of the prethermal plateau but not the duration of the phase.

*Outlook.*—We revealed a dynamical heating transition between a prethermal and an infinite-temperature phase in the limit of infinite times and drive frequencies. Its existence influences strongly the evolution of periodically-driven many-body spin chains even at the experimentally-relevant moderate frequencies and times. This becomes manifest in a long-lived prethermal phase, which can be modeled in a controllable fashion by an approximate effective nonlinear Floquet-Hamilton function derived using the inverse-frequency expansion. Contrary to naïve expectations, the prethermal phase is fused by drive-induced coherence, and is not a featureless thermal state.

Even though, a detailed comparison of thermalization in classical and quantum Floquet systems would be desirable, our analysis already presents compelling evidence that the prethermal phase, observed in a variety of quantum models, survives in the classical limit [54, 62]. This suggests that studies in cold atomic Floquet systems aiming to explain the contribution to heating due to higher bands or preparation of states under periodic driving, can be done (semi-)classically to reduce finite-size effects. In fact, our study directly relates to experimental platforms, such as shaken superfluid ultracold gases, where the physics is governed by a classical spin model [17], or photonic topological insulators [28–30], described by the nonlinear wave equation.

The results of our work pave the way for extending the powerful and creative ideas of Floquet engineering beyond the quantum realm over to classical many-

body systems. It opens up intriguing possibilities to translate tools, such as the Schrieffer-Wolff transformation for strongly-correlated quantum systems [63], in the language of canonical transformations, to reveal deeper analogies between quantum and classical mechanics. The existence of local quasi-conserved integrals of motion, obtained using the inverse-frequency expansion, raises the question about generalizing Floquet's theorem to nonlinear differential equations within the prethermal phase, which could have far-reaching consequences in biophysics and engineering.

*Acknowledgements.* — We thank Pankaj Mehta for interesting and insightful discussions. OH was supported by BU UROP student funding and the Simmons Foundation Investigator grant MMLS to Pankaj Mehta. DS acknowledges support from the FWO as post-doctoral fel-

low of the Research Foundation – Flanders and CMTV. AP and PW were supported by NSF DMR-1506340, AFOSR FA9550-16-1-0334 and ARO W911NF1410540. MB acknowledges support from the Emergent Phenomena in Quantum Systems initiative of the Gordon and Betty Moore Foundation and ERC synergy grant UQUAM. We used **QuSpin** for simulating the nonlinear EOM in the case of monochromatic drive [64]. The authors are pleased to acknowledge that the computational work reported on in this paper was performed on the Shared Computing Cluster which is administered by **Boston University's Research Computing Services**. The authors also acknowledge the Research Computing Services group for providing consulting support which has contributed to the results reported within this paper.

- 
- [1] N. Goldman and J. Dalibard, *Phys. Rev. X* **4**, 031027 (2014).
  - [2] A. Eckardt, *Rev. Mod. Phys.* **89**, 011004 (2017).
  - [3] M. Bukov, L. D'Alessio, and A. Polkovnikov, *Advances in Physics* **64**, 139 (2015).
  - [4] P. Kapitza, *Soviet Phys. JETP* **21**, 588 ((1951)).
  - [5] T. Oka and H. Aoki, *Phys. Rev. B* **79**, 081406 (2009).
  - [6] T. Kitagawa, T. Oka, A. Brataas, L. Fu, and E. Demler, *Phys. Rev. B* **84**, 235108 (2011).
  - [7] G. Jotzu, M. Messer, R. Desbuquois, M. Lebrat, T. Uehlinger, D. Greif, and T. Esslinger, *Nature* **515**, 237 (2014).
  - [8] M. Aidelsburger, M. Lohse, C. Schweizer, M. Atala, J. T. Barreiro, S. Nascimbène, N. R. Cooper, I. Bloch, and N. Goldman, *Nature Physics* **11**, 162 (2015).
  - [9] N. Fläschner, B. S. Rem, M. Tarnowski, D. Vogel, D.-S. Lühmann, K. Sengstock, and C. Weitenberg, *Science* **352**, 1091 (2016).
  - [10] M. Tarnowski, F. N. Ünal, N. Fläschner, B. S. Rem, A. Eckardt, K. Sengstock, and C. Weitenberg, *arXiv preprint arXiv:1709.01046* (2017).
  - [11] M. Tarnowski, M. Nuske, N. Fläschner, B. Rem, D. Vogel, L. Freystatzky, K. Sengstock, L. Mathey, and C. Weitenberg, *Phys. Rev. Lett.* **118**, 240403 (2017).
  - [12] M. Aidelsburger, S. Nascimbène, and N. Goldman, *arXiv preprint arXiv:1710.00851* (2017).
  - [13] G. Jotzu, M. Messer, F. Görg, D. Greif, R. Desbuquois, and T. Esslinger, *Phys. Rev. Lett.* **115**, 073002 (2015).
  - [14] J. Struck, C. Ölschläger, R. Le Targatn, P. Soltan-Panahi, A. Eckardt, M. Lewenstein, P. Windpassinger, and K. Sengstock, *Science* **333** (6045), 996 (2011).
  - [15] J. Struck, C. Ölschläger, M. Weinberg, P. Hauke, J. Simonet, A. Eckardt, M. Lewenstein, K. Sengstock, and P. Windpassinger, *Phys. Rev. Lett.* **108**, 225304 (2012).
  - [16] P. Hauke, O. Tieleman, A. Celi, C. Ölschläger, J. Simonet, J. Struck, M. Weinberg, P. Windpassinger, K. Sengstock, M. Lewenstein, and A. Eckardt, *Phys. Rev. Lett.* **109**, 145301 (2012).
  - [17] J. Struck, M. Weinberg, C. Ölschläger, P. Windpassinger, J. Simonet, K. Sengstock, R. Höppner, P. Hauke, A. Eckardt, M. Lewenstein, and L. Mathey, *Nature Physics* **9**, 738 (2013).
  - [18] M. Aidelsburger, M. Atala, M. Lohse, J. T. Barreiro, B. Paredes, and I. Bloch, *Phys. Rev. Lett.* **111**, 185301 (2013).
  - [19] H. Miyake, G. A. Siviloglou, C. J. Kennedy, W. C. Burton, and W. Ketterle, *Phys. Rev. Lett.* **111**, 185302 (2013).
  - [20] M. Atala, M. Aidelsburger, M. Lohse, J. T. Barreiro, B. Paredes, and I. Bloch, *Nature Physics* **10**, 588 (2014).
  - [21] C. J. Kennedy, W. C. Burton, W. C. Chung, and W. Ketterle, *Nature Physics* **11**, 859 (2015).
  - [22] V. Galitski and I. B. Spielman, *Nature* **494**, 49 (2013).
  - [23] K. Jiménez-García, L. J. LeBlanc, R. A. Williams, M. C. Beeler, C. Qu, M. Gong, C. Zhang, and I. B. Spielman, *Phys. Rev. Lett.* **114**, 125301 (2015).
  - [24] F. Görg, M. Messer, K. Sandholzer, G. Jotzu, R. Desbuquois, and T. Esslinger, *arXiv preprint arXiv:1708.06751* (2017).
  - [25] A. Celi, P. Massignan, J. Ruseckas, N. Goldman, I. B. Spielman, G. Juzeliūnas, and M. Lewenstein, *Phys. Rev. Lett.* **112**, 043001 (2014).
  - [26] B. Stuhl, H.-I. Lu, L. Ayccock, D. Genkina, and I. Spielman, *Science* **349**, 1514 (2015).
  - [27] M. Mancini, G. Pagano, G. Cappellini, L. Livi, M. Rider, J. Catani, C. Sias, P. Zoller, M. Inguscio, M. Dalmonte, *et al.*, *Science* **349**, 1510 (2015).
  - [28] M. C. Rechtsman, J. M. Zeuner, Y. Plotnik, Y. Lumer, D. Podolsky, F. Dreisow, S. Nolte, M. Segev, and A. Szameit, *Nature* **496**, 196 (2013).
  - [29] M. Hafezi, *Phys. Rev. Lett.* **112**, 210405 (2014).
  - [30] S. Mittal, J. Fan, S. Faez, A. Migdall, J. M. Taylor, and M. Hafezi, *Phys. Rev. Lett.* **113**, 087403 (2014).
  - [31] R. Desbuquois, M. Messer, F. Görg, K. Sandholzer, G. Jotzu, and T. Esslinger, *Phys. Rev. A* **96**, 053602 (2017).
  - [32] P. Weinberg, M. Bukov, L. D'Alessio, A. Polkovnikov, S. Vajna, and M. Kolodrubetz, *Physics Reports* (2017).
  - [33] V. Novičenko, E. Anisimovas, and G. Juzeliūnas, *Phys. Rev. A* **95**, 023615 (2017).
  - [34] M. Weinberg, C. Ölschläger, C. Sträter, S. Prella, A. Eckardt, K. Sengstock, and J. Simonet, *Phys. Rev. A* **92**, 043621 (2015).
  - [35] M. Reitter, J. Näger, K. Wintersperger, C. Sträter,

- I. Bloch, A. Eckardt, and U. Schneider, *Phys. Rev. Lett.* **119**, 200402 (2017).
- [36] S. Fishman, D. R. Grempel, and R. E. Prange, *Phys. Rev. Lett.* **49**, 509 (1982).
- [37] S. Lellouch, M. Bukov, E. Demler, and N. Goldman, *Phys. Rev. X* **7**, 021015 (2017).
- [38] S. Lellouch and N. Goldman, “Parametric instabilities in resonantly-driven bose-einstein condensates,” (2017), arXiv:1711.08832 .
- [39] L. D’Alessio and M. Rigol, *Phys. Rev. X* **4**, 041048 (2014).
- [40] Y. Bar Lev, D. J. Luitz, and A. Lazarides, *SciPost Physics* **3**, 029 (2017).
- [41] R. Moessner and S. Sondhi, *Nature Physics* **13**, 424 (2017).
- [42] R. Citro, E. G. Dalla Torre, L. D’Alessio, A. Polkovnikov, M. Babadi, T. Oka, and E. Demler, *Annals of Physics* **360**, 694 (2015).
- [43] K. Seetharam, P. Titum, M. Kolodrubetz, and G. Refael, *Phys. Rev. B* **97**, 014311 (2018).
- [44] D. A. Abanin, W. De Roeck, and F. Huveneers, *Phys. Rev. Lett.* **115**, 256803 (2015).
- [45] T. Mori, T. Kuwahara, and K. Saito, *Phys. Rev. Lett.* **116**, 120401 (2016).
- [46] M. Bukov, S. Gopalakrishnan, M. Knap, and E. Demler, *Phys. Rev. Lett.* **115**, 205301 (2015).
- [47] S. A. Weidinger and M. Knap, *Scientific reports* **7**, 45382 (2017).
- [48] E. Fermi, J. Pasta, S. Ulam, and M. Tsingou, *Los Alamos National Laboratory Document LA-1940* (1955).
- [49] S. F. C. Danieli, DK Campbell, “Intermittent fpu dynamics at equilibrium,” (2016), arXiv:1611.00434 .
- [50] N. N. Nekhoroshev, *Functional Analysis and Its Applications* **5**, 338 (1971).
- [51] J. Moser, *Math. Phys. K1 Ila* **nr.6** (1955), 87120 (1955).
- [52] J. Littlewood, *Proceedings of the London Mathematical Society* **3**, 343 (1959).
- [53] S. Notarnicola, F. Iemini, D. Rossini, R. Fazio, A. Silva, and A. Russomanno, *arXiv preprint arXiv:1709.05657* (2017).
- [54] R. Rajak, Atanu Citro and E. G. Dalla Torre, “Stability and pre-thermalization in chains of classical kicked rotors,” (2018), arXiv:1801.01142 .
- [55] G. Veble and T. Prosen, *Phys. Rev. Lett.* **92**, 034101 (2004).
- [56] G. Veble and T. Prosen, *Phys. Rev. E* **72**, 025202 (2005).
- [57] See Supplemental Material, which contains Ref. [64].
- [58] M. Bukov, M. Heyl, D. A. Huse, and A. Polkovnikov, *Phys. Rev. B* **93**, 155132 (2016).
- [59] P. W. Claeys and J.-S. Caux, *arXiv preprint arXiv:1708.07324* (2017).
- [60] P. W. Claeys, S. De Baerdemacker, O. E. Araby, and J.-S. Caux, *arXiv preprint arXiv:1712.03117* (2017).
- [61] F. Machado, G. D. Meyer, D. V. Else, C. Nayak, and N. Y. Yao, *arXiv preprint arXiv:1708.01620* (2017).
- [62] L. D’Alessio and A. Polkovnikov, *Annals of Physics* **333**, 19 (2013).
- [63] M. Bukov, M. Kolodrubetz, and A. Polkovnikov, *Phys. Rev. Lett.* **116**, 125301 (2016).
- [64] P. Weinberg and M. Bukov, *SciPost Phys.* **2**, 003 (2017).

## Supplemental Material

### I. ANALOGY OF THE DYNAMICAL HEATING TRANSITION WITH THE 1D ISING MODEL AT ZERO TEMPERATURE

The thermalization dynamics of the energy  $\langle Q(\ell T) \rangle$  and energy variance  $\langle \delta Q(\ell T) \rangle$  studied in this work are very similar in nature to the behavior of magnetization the one-dimensional Ising model close to zero temperature. Consider the 1d Ising energy function

$$\mathcal{H} = -J \sum_{j=1}^N \sigma_{j+1} \sigma_j, \quad (6)$$

where  $\sigma_j \in \{\pm 1\}$  are Ising variables and  $J$  is the interaction strength. This model is a paradigmatic example for a continuous phase transition between a magnetized and a disordered phase at zero temperature. Below, we discuss how this critical point affects the small but finite temperature physics, and draw an analogy to the dynamical heating phase transition reported on in the main text.

Figure 4 shows the expectation of the squared magnetization:  $M^2 = (N^{-1} \sum_i \sigma_i)^2$  and its variance as a function of the length of the chain  $N$  for different inverse temperatures  $\beta$ . The curves show a crossover when the system size becomes of order the correlation length which goes as  $\xi(\beta) \sim \exp(2J\beta)$ .

The scaling analysis for the heating transition described in the main text clearly exhibits the following scaling behaviour:

$$Q(\ell T, \Omega) = f_Q(\ell/l_{\text{scale}}(\Omega)), \quad (7)$$

with  $l_{\text{scale}}(\Omega) \sim \exp(c\Omega)$ , see Fig. 5. This bares a striking resemblance to the equilibrium finite size scaling in the 1d Ising chain:

$$\langle M^2(\beta, N) \rangle = f_{M^2}(N/\xi(\beta)). \quad (8)$$

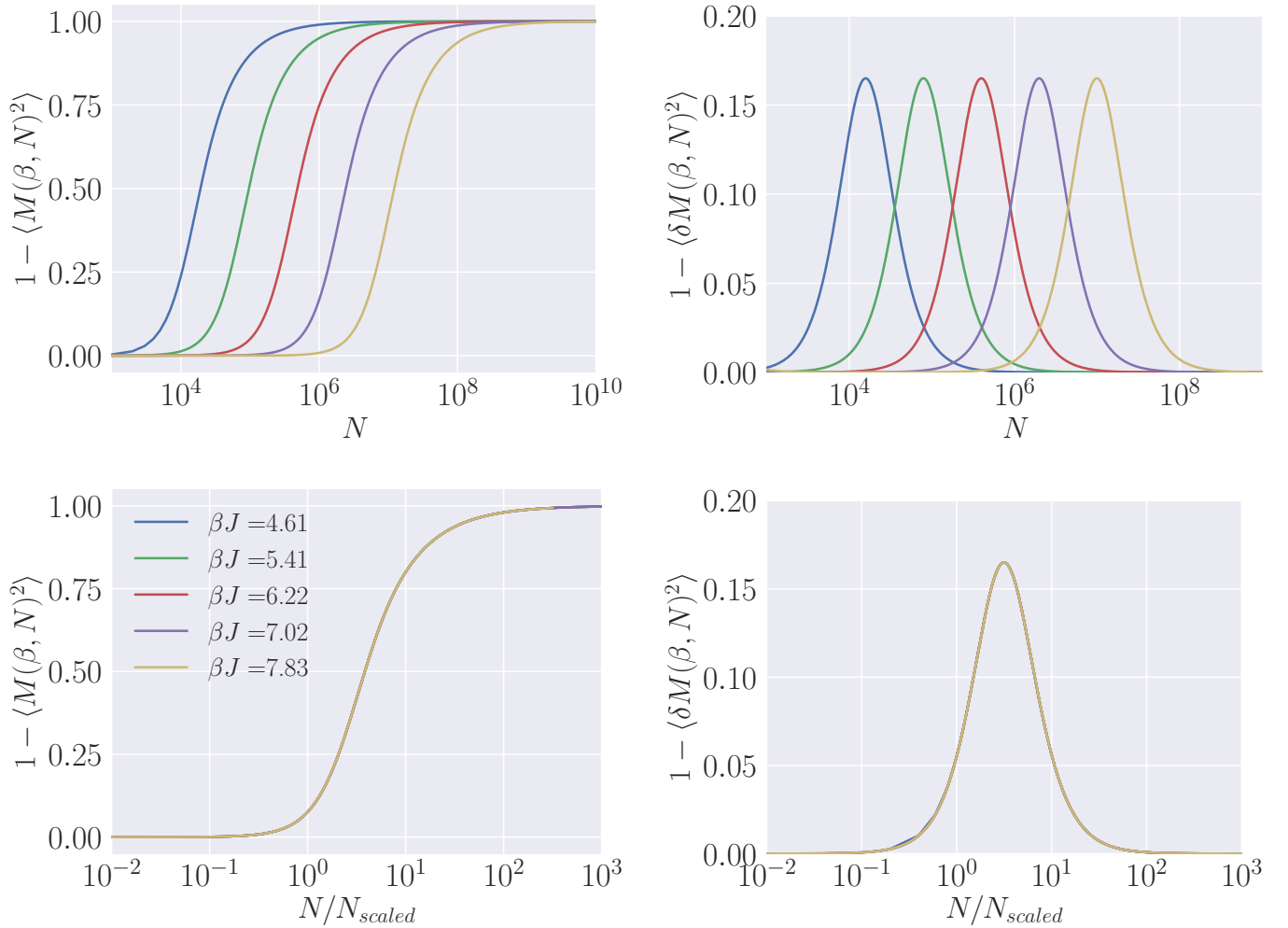


FIG. 4: The left plots show the behavior of the squared magnetization  $\langle M^2(\beta, N) \rangle$  for different inverse temperatures  $\beta$  as a function of the system size  $N$ . The right plots show the behavior of the variance of the squared magnetization  $\langle \delta M(\beta, N)^2 \rangle$ . The top panel on both sides shows the exact behavior while the bottom panel is rescaled with respect to the correlation length  $N_{\text{scaled}} = \xi(\beta)$  which is an exponential function of the inverse temperature. To be compared to Fig. 5.

Similar to defining a scaling time we can define a scaling length as  $N_{\text{scaled}} = \xi(\beta)$ . This suggests that for the heating transition,  $\Omega$  plays the role of  $\beta$ . At the same time, the correlation length,  $\xi(\beta) = N_{\text{scaled}}$ , is analogous to the time needed to begin the unconstrained thermalization process. Furthermore this analogy gives a very strong evidence for a dynamical phase transition at  $\Omega, t \rightarrow \infty$  as both the time dependent model and the equilibrium model share the same scaling behavior.

## II. TIME EVOLUTION OF THE STAGGERED MAGNETIZATION

Figure 6 shows the time-evolution of the magnetization for different frequencies, starting from the ground state of the period-averaged Hamiltonian  $H_{\text{ave}}$ . Each data point is averaged over 50 noise realizations. For low frequencies the mean magnetization exhibits prethermal plateaus that eventually decay to zero. This decay originates from the breakdown of the anti-ferromagnetic structure of the initial state. Figure 7 shows the behavior of the staggered magnetization for a single realization. In this case the magnetization exhibits spin flips which appear sharp even on a linear scale. These processes reveal the physical mechanism behind the onset of heating, which is associated with the proliferation of spin flips towards the end of the exponentially long-lived prethermal phase. For moderate-to-high frequencies these magnetization plateaus persist for the entire duration of the prethermal phase.

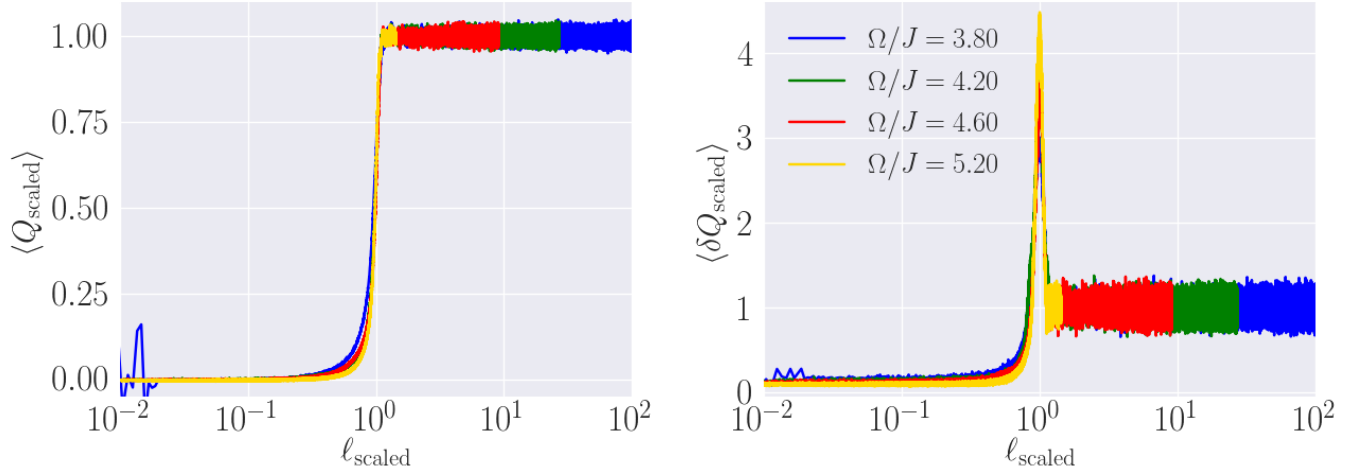


FIG. 5: Noise-averaged energy  $\langle Q(\ell T) \rangle$  and energy variance  $\langle \delta Q(\ell T) \rangle$  as a function of the rescaled number of driving cycles  $\ell_{\text{scaled}}$ . The simulation parameters are  $h/J = 0.809$ ,  $g/J = 0.9045$ . To be compared to Fig. 4.

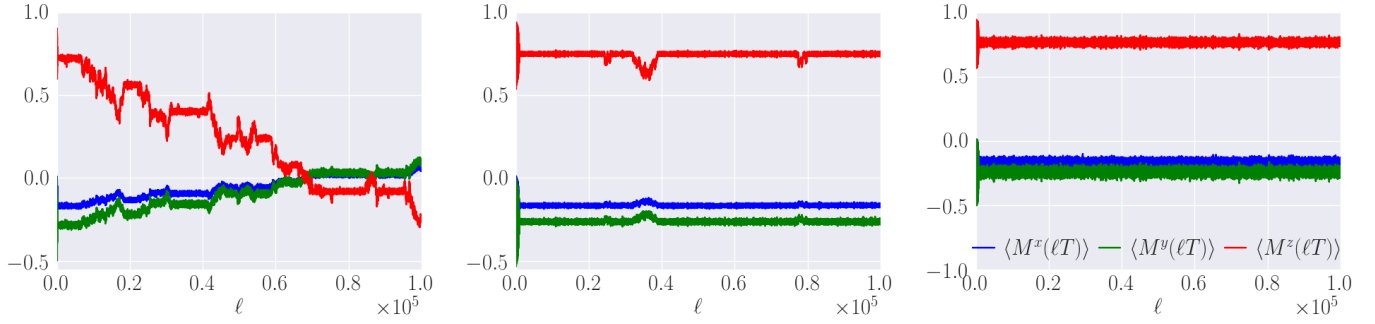


FIG. 6: The components of the staggered magnetization  $\langle M^\alpha(\ell T) \rangle$  as a function of the number of driving cycles  $\ell$ , for  $\Omega/J = 3.8$  (left),  $\Omega/J = 4.2$  (middle) and  $\Omega/J = 4.6$  (right). Each data point is averaged over 50 noise-realizations. The simulation parameters are  $h/J = 0.809$ ,  $g/J = 0.9045$ , and  $N = 100$ .

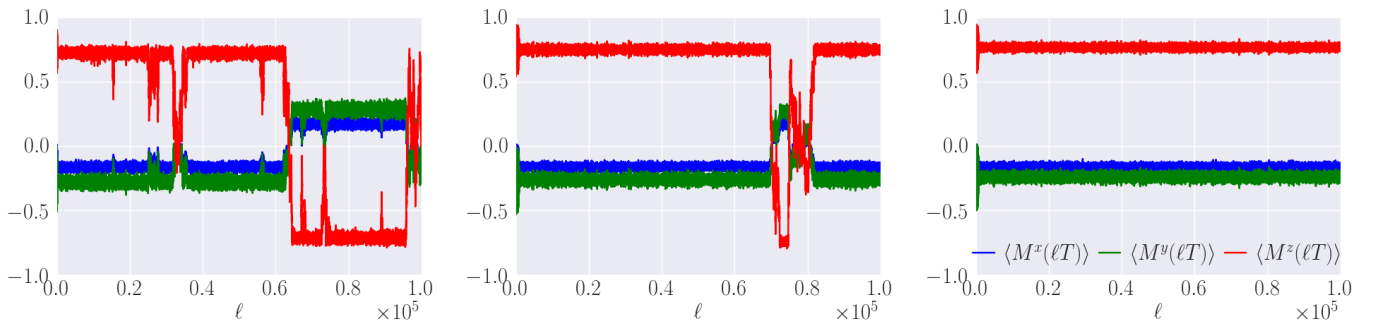


FIG. 7: A single noise realization showing the components of the staggered magnetization  $\langle M^\alpha(\ell T) \rangle$  as a function of the number of driving cycles  $\ell$ , for  $\Omega/J = 3.8$  (left),  $\Omega/J = 4.2$  (middle) and  $\Omega/J = 4.6$  (right). The simulation parameters are  $h/J = 0.809$ ,  $g/J = 0.9045$ , and  $N = 100$ .

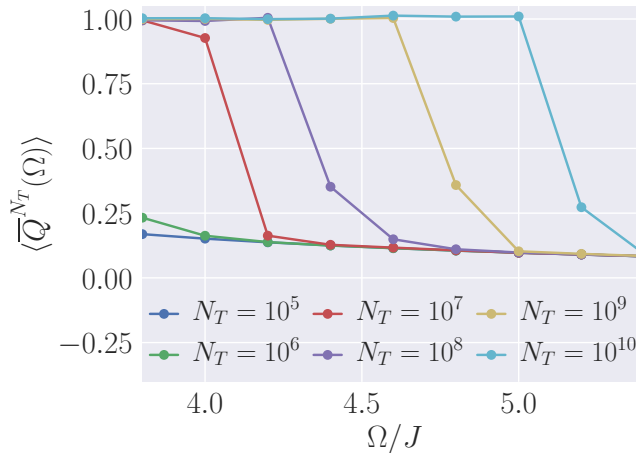


FIG. 8: Decade averaged energy absorption  $\langle \bar{Q}^{N_T}(\Omega) \rangle$  for six different decades as a function of the driving frequency  $\Omega/J$ . Each average is taken over 1000 periods. The simulation parameters are  $h/J = 0.809$ ,  $g/J = 0.9045$ , and  $N = 100$ .

### III. FREQUENCY DEPENDENCE OF ENERGY ABSORPTION

Often times one is interested in the averaged amount of energy absorbed from the drive. To measure this let us define the following time-averaged energy absorption, averaged at a given decade over 1000 periods

$$\langle \bar{Q}^{N_T}(\Omega) \rangle = \frac{1}{N_T} \sum_{\ell=N_T}^{N_T+1000} \langle \bar{Q}(\ell T; \Omega) \rangle, \quad (9)$$

where  $N_T$  denotes the number of driving cycles used for the long-time average. Theoretically, one would like to do the period averaging over infinitely many cycles,  $N_T \rightarrow \infty$ . However, in classical systems this is not possible. Therefore, we study the heating dependence as a function of frequency, for a sequence of exponentially growing time spans.

The existence of the heating transition at  $\Omega \rightarrow \infty$  and  $\ell \rightarrow \infty$  suggests that the infinite-temperature plateau of  $\langle \bar{Q}^{N_T}(\Omega) \rangle$  shifts to higher frequencies with increasing waiting time  $N_T$ . Figure 8 shows  $\langle \bar{Q}^{N_T}(\Omega) \rangle$  over seven consecutive decades in  $N_T$ . In agreement with theory, as  $N_T$  is increased the energy curves shift gradually to the right. Interestingly, the crossover region between the infinite-temperature and the prethermal phases sharpens very slowly which suggests some kind of logarithmic corrections to the finite time scaling.

### IV. DERIVATION OF THE EFFECTIVE FLOQUET-HAMILTON FUNCTION USING THE INVERSE-FREQUENCY EXPANSION

The cornerstone of Floquet theory in physics is Floquet's theorem. However, the theorem applies to *linear* ordinary differential equations, and hence its consequence become invalid for systems featuring nonlinear dynamics. On the other hand, chaos and thermalization are intimately tied to the nonlinearities in the Hamilton equations of motion. Therefore, finding effective descriptions for classical periodically-driven many-body systems is a challenging and difficult problem, and there might not exist a simple universal solution.

In periodically-driven quantum systems, the linearity of the Schrödinger equation fulfils the criteria for the applicability of Floquet's theorem. According to the latter, the evolution operator  $U(t, 0)$  factorizes as

$$\hat{U}(t, 0) = \mathcal{T}_t \exp \left( -i \int_0^t dt' \hat{H}(t') \right) = \hat{P}(t) e^{-it\hat{H}_F}, \quad (10)$$

with the so-called time-periodic micromotion operator  $\hat{P}(t) = \hat{P}(t + T)$ , which governs the fast intraperiod dynamics, and the effective time-independent Floquet Hamiltonian  $\hat{H}_F$ . Stroboscopically, the time evolution of the system is therefore described by the Floquet Hamiltonian  $\hat{H}_F$ .

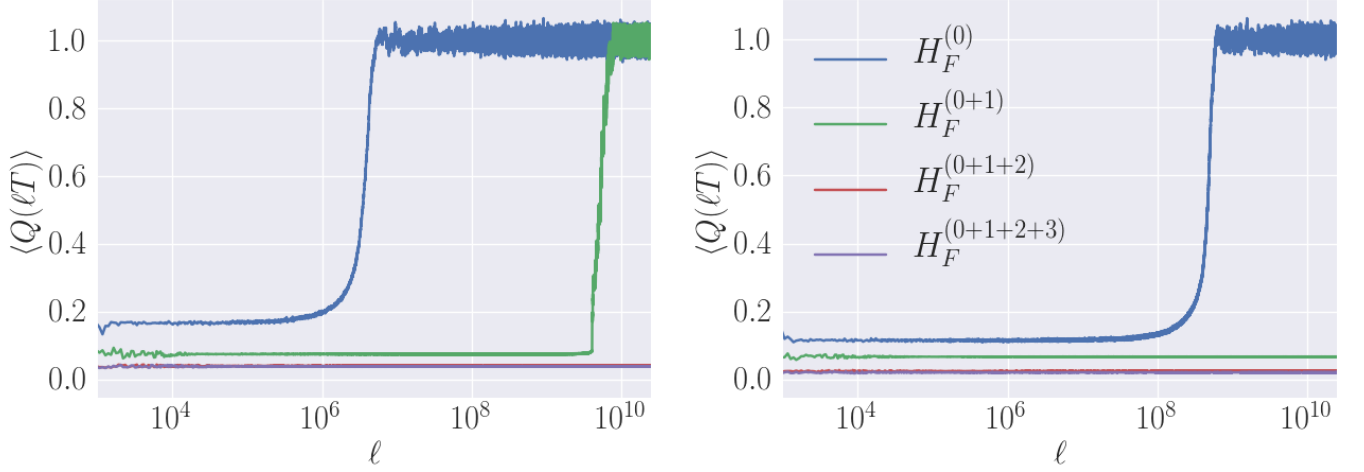


FIG. 9: Average energy absorption  $\langle Q(t) \rangle$  as a function of the number of driving cycles  $\ell$ , for different  $H_F^{(0+1+2+\dots k)}$  for  $k \in [0, 1, 2, 3]$ . The evolution is started in the ground state of  $H_F^{(0+1+2+\dots k)}$ . The frequency values are  $\Omega/J = 3.8$  (left) and  $\Omega/J = 4.6$  (right). The simulation parameters are  $h/J = 0.809$ ,  $g/J = 0.9045$ , and  $N = 100$ . Higher order terms absorb less energy after the initial quench and exhibit less fluctuations in the prethermal phase.

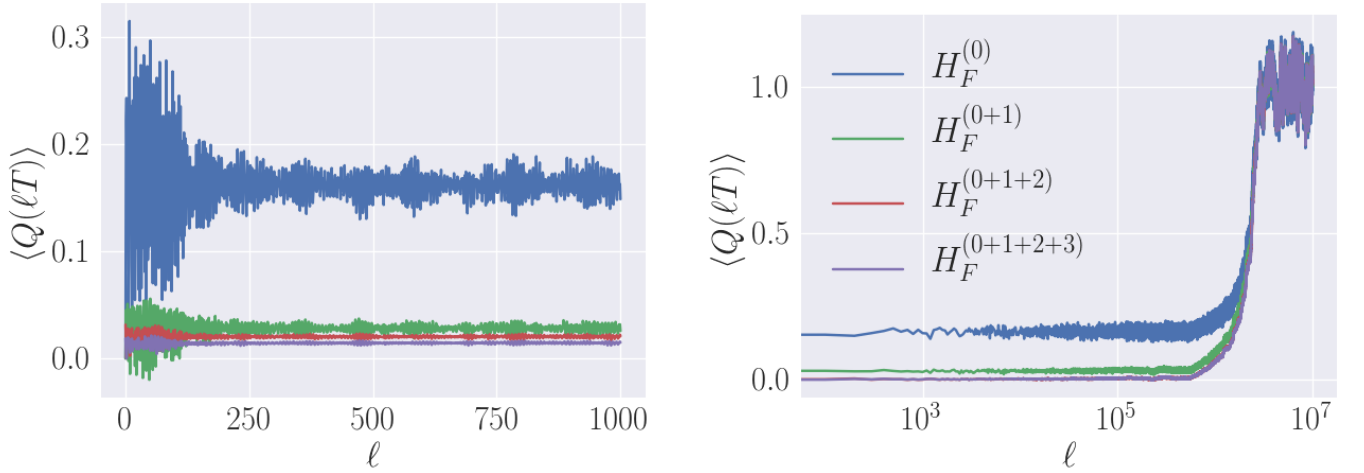


FIG. 10: Average energy absorption  $\langle Q(t) \rangle$  as a function of the number of driving cycles  $\ell$ , for different  $H_F^{(0+1+2+\dots k)}$  for  $k \in [0, 1, 2, 3]$ . The evolution is started in the ground state of  $H_F^{(0)}$  for all curves. The frequency value is  $\Omega/J = 3.8$ . The simulation parameters are  $h/J = 0.809$ ,  $g/J = 0.9045$ , and  $N = 100$ . Note that when started in  $H_F^{(0)}$  all Floquet expansions thermalize after the same number of periods but the evolution of higher order Floquet terms exhibit less fluctuations after the initial quench and in the prethermal phase.

The starting point in quantum Floquet theory is the assumption that the Floquet Hamiltonian can be expanded in a Taylor series in the inverse frequency

$$H_F = \sum_{n=0}^{\infty} H_F^{(n)}, \quad H_F^{(n)} \sim \mathcal{O}(\Omega^{-n}), \quad H_F^{(0+\dots+m)} = \sum_{n=0}^m H_F^{(n)}. \quad (11)$$

Combining this with Eq. (10), one can arrive at the inverse-frequency expansion for the Floquet Hamiltonian, see Refs. [1–3] for more details. A notable advantage of these expansions is that they remain valid beyond the linear response regime, and allow to study strongly driven systems.

Let us apply the Magnus expansion – one of the variants of the inverse-frequency expansion – to the step-driven

spin chain. Note that if we write the Hamiltonian as

$$\hat{H}(t) = \begin{cases} \hat{A} & \text{for } t \in [0, T/2] \bmod T \\ \hat{B} & \text{for } t \in [T/2, T] \bmod T \end{cases}$$

where

$$\hat{A} = \sum_{j=1}^N J \hat{S}_j^z \hat{S}_{j+1}^z + h \hat{S}_j^z, \quad \hat{B} = \sum_{j=1}^N g \hat{S}_j^x, \quad (12)$$

the time evolution operator takes the form

$$\hat{U}(T, 0) = \exp(-i\hat{H}_F T) = \exp\left(-i\hat{B}\frac{T}{2}\right) \exp\left(-i\hat{A}\frac{T}{2}\right). \quad (13)$$

For this setup, applying the Magnus expansion is equivalent to the Baker-Campbell-Hausdorff formula, which to third order in the inverse frequency gives:

$$\begin{aligned} \hat{H}_{\text{ave}} = \hat{H}_F^{(0)} &= \frac{1}{2}(\hat{A} + \hat{B}), \\ \hat{H}_F^{(1)} &= \frac{T}{8}[\hat{B}, \hat{A}], \\ \hat{H}_F^{(2)} &= \frac{T^2}{96}\left([\hat{B}, [\hat{B}, \hat{A}]] + [\hat{A}, [\hat{A}, \hat{B}]]\right), \\ \hat{H}_F^{(3)} &= -\frac{T^3}{284}[\hat{A}, [\hat{B}, [\hat{B}, \hat{A}]]]. \end{aligned} \quad (14)$$

In Ref. [3] it was noted that if we formally replace the commutator  $[\cdot, \cdot]$  by the Poisson bracket  $\{\cdot, \cdot\}$ , the expansion translates over to classical systems. In our model, this leads to

$$\begin{aligned} H_F^{(0)} &= \frac{1}{2} \sum_{j=1}^N J S_j^z S_{j+1}^z + h S_j^z + g S_j^x, \\ H_F^{(1)} &= \frac{-gT}{8} \sum_{j=1}^N (J(S_{j+1}^z + S_{j-1}^z) + h) S_j^y, \\ H_F^{(2)} &= \frac{T^2}{96} \sum_{j=1}^N J g^2 (S_j^y (S_{j+1}^y + S_{j-1}^y) - S_j^z (S_{j+1}^z + S_{j-1}^z)) - g^2 h S_j^z \\ &\quad - J g S_j^x S_{j+1}^z (J(S_{j+1}^z + S_{j-1}^z) + h) - J g S_{j+1}^x S_j^z (J(S_{j+2}^z + S_j^z) + h) - g h (J(S_{j+1}^z + S_{j-1}^z) + h) S_j^x, \\ H_F^{(3)} &= \frac{T^3}{284} \sum_{j=1}^N J g^2 h S_j^x (S_{j+1}^z + S_{j-1}^z) + J^2 g^2 S_{j+1}^x S_j^x (S_{j+1}^z + S_{j-1}^z) + J^2 g^2 S_j^x S_{j+1}^x (S_{j+2}^z + S_j^z). \end{aligned} \quad (15)$$

The above approach is equivalent to starting from a classical periodically-driven system, quantizing it, applying the Magnus expansion, and then taking the classical limit. While this procedure is straightforward to apply, the absence of Floquet's theorem for classical chaotic systems casts doubt on how controlled the expansion is. Figure 9 shows a comparison between the different order Magnus expansion for energy absorption [see main text for a comparison on the staggered magnetization]. For every order  $m$  in the Magnus expansion, we start from the GS of the corresponding approximate classical Floquet-Hamilton function  $H_F^{(0+\dots+m)}$ . It can be completely defined on a two site unit cell. Except for  $m > 0$  we have a nonzero  $S_j^y$  component, induced by the  $y$ -field in the first-order Floquet-Hamilton function. To find the correct ground state, we parametrize the spin vector  $\vec{S}_j$  by spherical coordinates  $(\theta_j, \phi_j)$ ,  $j = 1, 2$ , and variationally determine the angles. The true ground state must thus be solved for numerically. Note that the ground state for  $m > 0$  is also dependent on the driving frequency  $\Omega$ . We then evolve the initial state with the exact time-dependent Hamilton function  $H(t)$ , and measure the energy  $H_F^{(0+\dots+m)}$ .

Starting from the GS of the corrected Hamiltonian, we find that the higher-order terms have the following salient effects, see Fig. 9. Firstly, the initial energy fluctuations arising from the ferromagnetic structure of the ground state during the constrained thermalization in stage (i) are reduced. In addition, the unconstrained thermalization transient (iii) shows a sharper transition with increasing the order of the expansion. For comparison, we also kept the initial GS to be fixed as the GS of  $H_F^{(0)}$ , and repeated the procedure, see Fig. 10. Clearly, while the pre-thermal plateau is reduced with increasing the order of the expansion, the heating time scale remains unchanged.

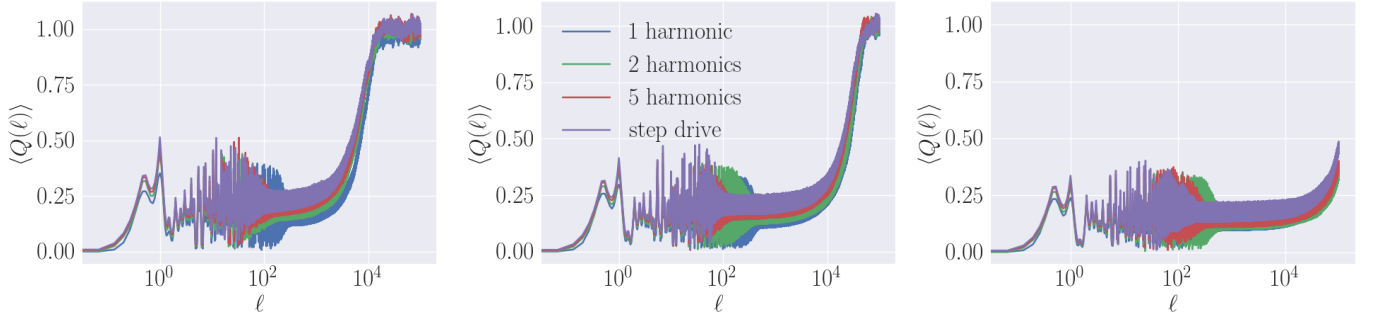


FIG. 11: Average energy absorption  $\langle Q(t) \rangle$  as a function of the number of driving cycles  $\ell$  for different truncations of  $f(t)$ . The graphs shown have  $\Omega/J = 3.0$  (left),  $\Omega/J = 3.2$  (middle) and  $\Omega/J = 3.4$  (right). The simulation parameters are  $h/J = 0.809$ ,  $g/J = 0.9045$ , and  $N = 100$ . This plot shows 15 points per period not just stroboscopic dynamics.

## V. MONO- VS POLYCHROMATIC DRIVES. THE EFFECT OF MICROMOTION.

Throughout this study we used a time-periodic step drive function. This was a key property which ultimately allows us to reach astronomically long times. However, typically in experiments it is easier to apply periodic modulations with few harmonics, while step drives require more precise apparatus. One may, therefore, wonder how the heating properties of the system might change, if we used few-harmonic drives instead.

Here, we give evidence that the form of the drive is relatively unimportant when considering the qualitative behavior of thermalizing dynamics. Let us cast the Hamilton function in the generalized form

$$H(t) = \frac{1}{2}(A + B) + \frac{f(t)}{2}(A - B), \quad (16)$$

see Eq. (12). For a step drive, we can Fourier-decompose the protocol as follows

$$f(t) = \frac{4}{\pi} \sum_{n=1}^{\infty} \frac{1}{2n-1} \sin((2n-1)\Omega t) = \begin{cases} +1 & \text{for } t \in [0, T/2] \bmod T \\ -1 & \text{for } t \in [T/2, T] \bmod T \end{cases} \quad (17)$$

Note that each term of the expansion of  $f(t)$  has zero average over a period. Thus, no matter the number of terms at which the series is truncated,  $H_F^{(0)} = \frac{1}{2}(A + B)$ .

Figure 11 shows a comparison of the energy absorption with  $f(t)$  truncated at different orders in the Fourier expansion. The graphs show that the presence of higher order Fourier modes only marginally increases the rate of heating throughout the frequency range of interest. Hence, the picture developed in the main text about the properties of the thermalizing dynamics remain robust to the number of harmonics the driving protocol is composed of. Furthermore, this graphs the behavior for all times not just stroboscopically. This suggests that no matter the Floquet gauge chosen the qualitative behavior of system is the same. We used QuSpin [64] to simulate the nonlinear EOM.

## VI. SYSTEM SIZE DEPENDENCE

Figure 12 shows that for large system sizes the timescale at which the prethermal phase ends and thermalisation occurs is the same. However, the steepness of this heating process increases with the system size. Additionally, in the infinite-temperature state, stage (iv), reaching larger system sizes reduces the size of the energy fluctuations, as anticipated from the laws of Statistical Mechanics.

## VII. STABILITY OF THE NUMERICAL INTEGRATION OF THE HAMILTON EQUATIONS

The Hamilton EOM for our model can be solved using an analytic recursion relation during in each half period [see main text]. This means that the stroboscopic evolution of the system is described by a iterative application of a discrete nonlinear map. Iterative recursive relations are easier to simulate numerically than a system of time-dependent non-linear differential equations.

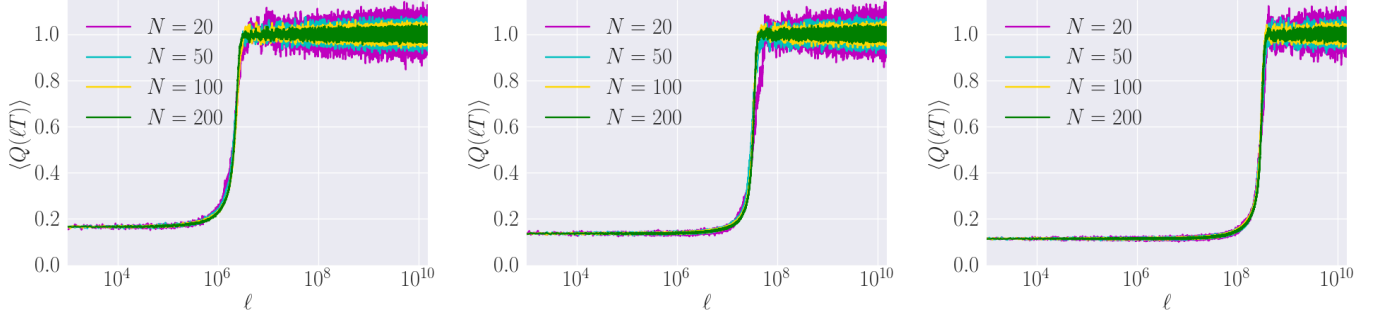


FIG. 12: Average energy absorption  $\langle Q(t) \rangle$  as a function of the number of driving cycles  $\ell$  for system sizes  $N = 20, 50, 100, 200$ . The graphs shown have driving frequencies  $\Omega/J = 3.8$  (left),  $\Omega/J = 4.2$  (middle) and  $\Omega/J = 4.6$  (right). The simulation parameters are  $h/J = 0.809$ ,  $g/J = 0.9045$ . Note how the fluctuations decrease with system size while the steepness increases with system size.

Nevertheless, when we deal with times as large as  $10^{10}$  driving cycles, it is imperative to ensure that the numerical error growth is under control at all times. To test it, recall that the spin algebra requires that the squared on-site magnetization

$$C_j(\ell T) = |\vec{S}_j(\ell T)|^2 \quad (18)$$

is an integral of the motion. In particular, it is fixed to unity for every lattice site and at all times. The origin of this integral of motion can be traced back to the Casimir operator of the spin algebra.

The relative error in  $C_j(\ell T)$  represents a reliable measure of how large the numerical integration error is. Since the squared magnetization is defined for each lattice site, an absolute value for the error is given by the maximum deviation over the entire chain:

$$C(\ell T) = \max_j |C_j(\ell T) - 1| \quad (19)$$

Figure 13 shows the time-dependence of  $C(\ell T)$ . One can see that the maximum error is no bigger than  $10^{-5}$  at the end of the time evolution. This is a good indicator that the numerical simulation is sufficiently accurate to render our analysis reliable. Indeed, note that (exponential) blow up of the curves due to numerical error happens at times order of magnitudes larger than stage (iii), during which unconstrained thermalization to an infinite-temperature state occurs for a given frequency.

For comparison, the average error  $N^{-1} \sum_{j=1}^N |C_j(\ell T) - 1| \sim 10^{-10}$  is a few orders of magnitude smaller, due to self-averaging effects.

### VIII. DEPENDENCE ON THE SIZE OF THE NOISE DISTRIBUTION FOR THE INITIAL STATE.

As we explained in the main text, in order to make our results robust to the chaotic character of the many-body dynamics, we add small noise in the azimuthal angle of the initial antiferromagnetic state. By studying the long time behavior of energy absorption, here we show that the size of the support of the noise distribution is irrelevant to the qualitative picture of the thermalizing dynamics. Figure 14 shows the time-dependent of the energy absorption for three different values for the support of the uniform noise distribution:  $[-\pi/W, \pi/W]$ , with  $W \in \{50, 150, 500\}$ .

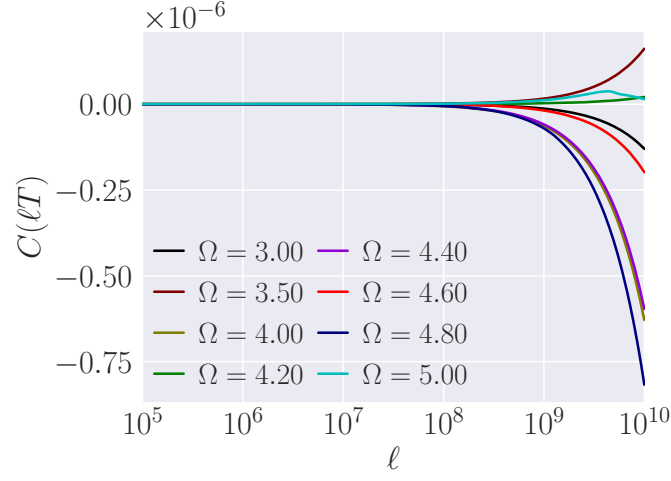


FIG. 13: The maximum error of the Casimir operator  $C(\ell T)$  as a function of the number of driving cycles  $\ell$  for different  $\Omega/J$  values. The simulation parameters are  $h/J = 0.809$ ,  $g/J = 0.9045$ , and  $N = 100$ .

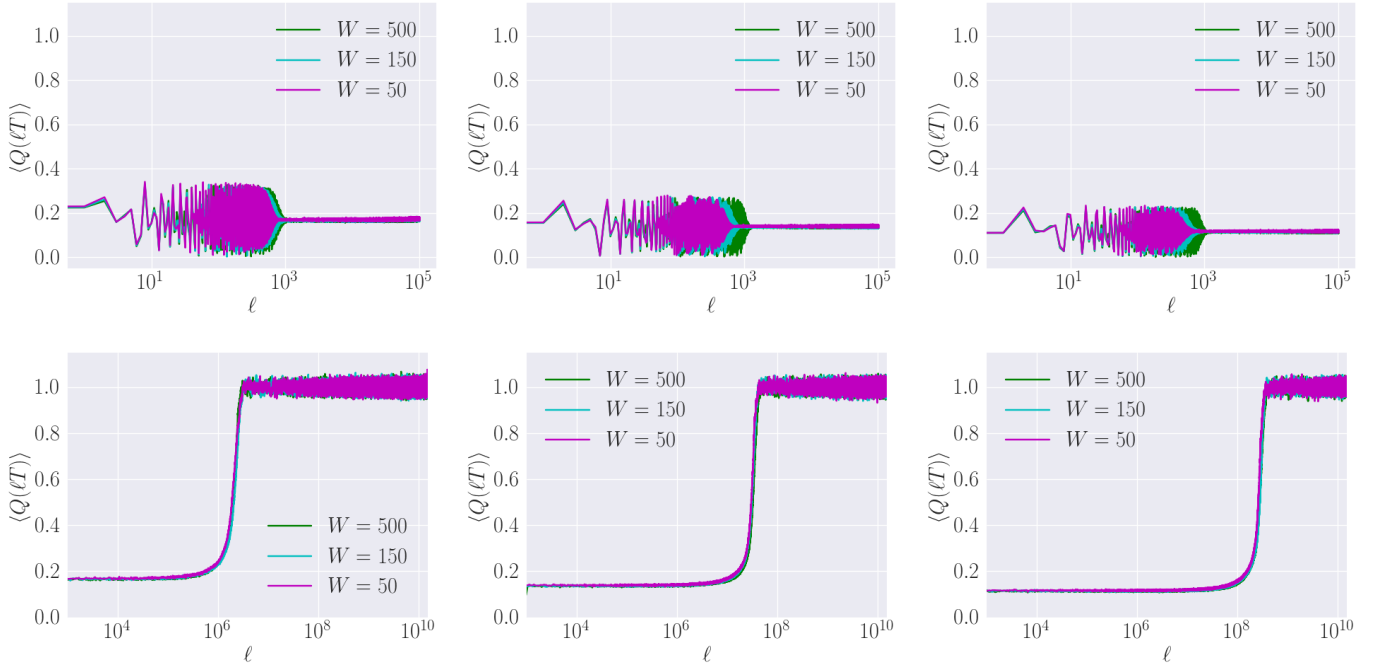


FIG. 14: Average energy absorption  $\langle Q(t) \rangle$  as a function of the number of driving cycles  $\ell$ , for  $\Omega/J = 3.8$  (left),  $\Omega/J = 4.2$  (middle) and  $\Omega/J = 4.6$  (right). The above panels show the initial fluctuations due to two particle behavior and the lower show behavior for long times. The  $W$  value corresponds to the strength of the initial noise. The simulation parameters are  $h/J = 0.809$ ,  $g/J = 0.9045$ , and  $N = 100$ .